

## Electronic properties of 4-nm FePt particles

B. Stahl,<sup>1,\*</sup> J. Ellrich,<sup>1</sup> R. Theissmann,<sup>1</sup> M. Ghafari,<sup>1</sup> S. Bhattacharya,<sup>1</sup> H. Hahn,<sup>1</sup> N. S. Gajbhiye,<sup>2</sup> D. Kramer,<sup>3</sup>  
R. N. Viswanath,<sup>3</sup> J. Weissmüller,<sup>3</sup> and H. Gleiter<sup>3</sup>

<sup>1</sup>Fachbereich Material- und Geowissenschaften, Petersenstrasse 23, TU Darmstadt, 64287 Darmstadt, Germany

<sup>2</sup>Department of Chemistry, Indian Institute of Technology Kanpur, Uttar Pradesh 208 016, India

<sup>3</sup>Institut für Nanotechnologie, Forschungszentrum Karlsruhe, D-76021 Karlsruhe, Germany

(Received 19 August 2002; revised manuscript received 6 November 2002; published 31 January 2003)

The structural, electronic and magnetic properties of 4 nm metallic FePt particles were studied by X-ray diffraction (XRD), Rutherford backscattering spectroscopy (RBS), transmission electron microscopy (TEM), X-ray photo electron spectroscopy (XPS), magnetometry and Mössbauer spectroscopy. At low temperatures, the Mössbauer data reveal an unusually high and well defined magnetic hyperfine field compared to FePt multilayer or bulk samples. The magnetic anisotropy of the as-prepared FePt particles embedded in a layer of oleic acid molecules arises from surface contributions. The distribution of anisotropy under the constraint of a constant particle moment and volume is reflected in the hysteresis loop as a function of external field at 4.3 K. Due to faceting as seen in the high resolution TEM images, the magnetization reversal does not follow the simple Stoner-Wohlfarth switching. The annealing experiments show that at a size of 4 nm the high-temperature fcc phase is stable up to at least 560 °C as long as agglomeration and particle growth is prevented.

DOI: 10.1103/PhysRevB.67.014422

PACS number(s): 75.50.Tt, 71.20.Be, 73.22.Dj, 75.50.Ss

### I. INTRODUCTION

The concept of metallic behavior is based on the translational invariance of an infinite crystal. Nevertheless, metallic properties are conserved down to very small geometrical dimensions.<sup>1,2</sup> For instance, Au particles as small as 3 nm exhibit metallic reflectivity.<sup>3,4</sup> However, collective electronic excitations change their characteristic parameters like the resonance frequency and lifetime.<sup>5</sup> This is the origin of color variations as a function of Au particle size. In small metallic particles the surface plays a crucial role in determining the electronic properties of the whole particle.<sup>6</sup> Due to the enhanced reactivity of metallic nanoparticles oxide coatings are readily formed. Even noble metals like Au can be highly reactive as atoms or nanoparticles.<sup>7,8</sup> This complicates the interpretation of physical measurements as it is not easy to distinguish between the signals of the coating and the core. In addition, the coating can substantially change the properties of the core<sup>9,10</sup> which for instance leads in magnetic systems to exchange biasing effects<sup>11,12</sup> or changes in the magnetic moment.<sup>13,14</sup> It has been shown that a decoration of the nanoparticle's surface with organic ligands can help to prevent oxidation. Nevertheless, subtle changes in the chemistry of the ligands can have dramatic effects on the electronic properties of the nanoparticle.<sup>15-17</sup> In Au<sub>55</sub> clusters<sup>18,19</sup> a metal-insulator transition is observed when decorating the surface with 6 Cl atoms in addition to a shell of 12 triphenylphosphine molecules.<sup>20</sup> Another way of studying pure metal clusters is to produce them in ultrahigh vacuum and characterize them *in situ*. Though this strongly limits the number of applicable measuring techniques, features like the magic numbers of atoms, enhanced magnetic moments per atom,<sup>21-25</sup> and ferromagnetism in Rh,<sup>14,26,27</sup> a nonmagnetic material in bulk form, are observed.

In this paper we focus on a comprehensive study of 4-nm FePt particles as a model alloy system that shows surprising structural, electronic,<sup>28</sup> and magnetic features.<sup>29,30</sup> The expla-

nation of the observed properties can only be found in a subtle interplay of alloying, finite size, and surface contributions to the electronic structure of the metallic system. FePt nanoparticles have already been produced by Sun *et al.*<sup>31</sup> by a wet chemical technique (the polyol process<sup>32</sup>) that results in particles covered by a shell of organic ligands. This morphology enables the preparation of self-organized two- and three-dimensional arrays of these monodisperse nanoparticles. A structural transition from a disordered fcc alloy to an ordered fct intermetallic phase upon annealing at 550 °C was reported. Our aim is to clarify the electronic and thus magnetic properties of this system under different conditions. Of special interest is the influence of the surface chemistry on the electronic system.

### II. SYNTHESIS

In the same way as in the initial work by Sun *et al.*<sup>31</sup> and described in more general terms by Mulvaney *et al.*,<sup>3</sup> FePt nanoparticles were synthesized by wet chemical processing under N<sub>2</sub> atmosphere. Platinum acetylacetonate [Pt(acac)<sub>2</sub>] and iron pentacarbonyl [Fe(CO)<sub>5</sub>] were used as precursors. During the reaction process the evaporating fraction of Fe(CO)<sub>5</sub> was condensed in a water cooled glass tube and recycled to the reaction zone. Figure 1 gives an overview over the principal synthesis process in which only a thermal

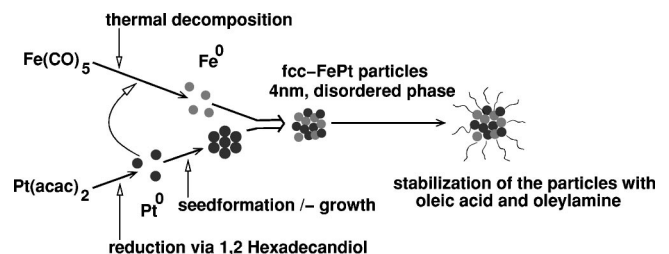


FIG. 1. Synthesis route of 4-nm FePt particles by wet chemistry.

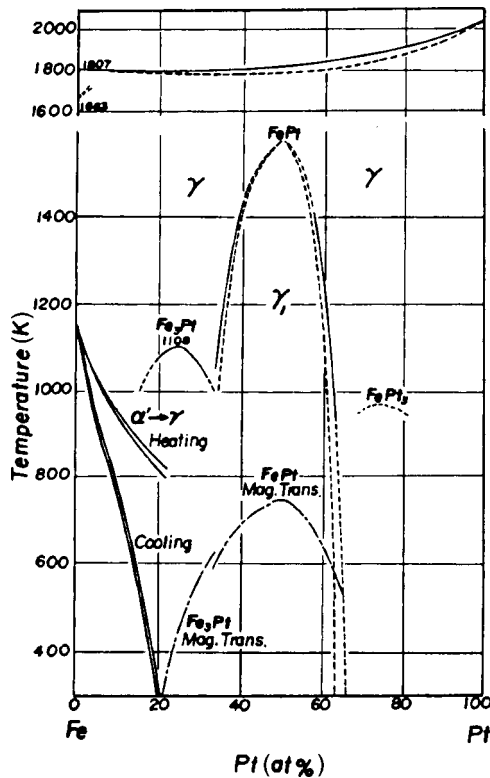


FIG. 2. Bulk phase diagram of the Fe-Pt system (Refs. 33 and 34).

decomposition of the iron precursor is considered. It is quite possible that in the presence of Pt atoms and clusters the decomposition of the iron precursor is already catalyzed at lower temperatures.

As will be outlined later, the FePt nanoparticles coated with a monomolecular layer of oleic acid are stable against oxidation in air. This allows for an easy handling of the material in air in order to prepare the samples for the different characterization techniques.

### III. EXPERIMENTAL RESULTS

The experiments that were carried out sought to answer the following crucial questions on the FePt nanoparticles:

- (i) What is the average stoichiometry of the particles?
- (ii) What is their shape, size distribution, and crystal structure? Can agglomeration be excluded?
- (iii) How are Fe and Pt distributed within the particles? Do they exhibit a core-shell structure?
- (iv) Can oxidation of the particles be excluded?
- (v) What are the intrinsic electronic properties of these supposedly metallic particles?
- (vi) How are the electronic properties reflected in the magnetic behavior? What are the core and shell contributions to the magnetic anisotropy?

As the Fe-Pt system shows a multitude of intermetallic as well as magnetic phases the precise knowledge of the stoichiometry is essential (Fig. 2). The average Fe-Pt ratio can be determined with high precision by Rutherford backscattering spectroscopy (RBS). Since the backscattering yield is com-

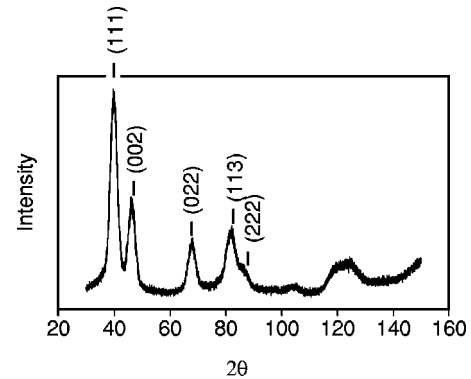


FIG. 3. X-ray-diffraction pattern of the as-prepared sample, batch I.

pletely determined by Coulomb scattering of the projectiles (2-MeV  $\alpha$  particles) by the Fe or Pt nuclei, the chemistry and morphology of the sample do not influence the result. The analysis of the step height of the Fe and Pt edge in the RBS spectrum gives an Fe fraction of 50.2(2)%. According to the bulk phase diagram the system should be in a ferromagnetic state below 750 K. Above 1580 K the ordered  $\gamma_1$  phase (fcc) transforms into the disordered  $\gamma$  phase (fcc).

#### A. Crystallographic structure

The Rietveld analysis of the x-ray-diffraction data (Fig. 3) of the as-prepared particles reveal the fcc structure of the sample with a lattice constant of 0.3839(2) nm. This is confirmed by the small area electron diffraction pattern (SAED) in the TEM [Fig. 4(c)]. No superstructure peaks were found which is characteristic for the disordered alloy. The high-resolution TEM image of a single particle in Fig. 4(b) demonstrates the faceted morphology. 20 atomic layers are resolved between the two arrows. The spacing of the lattice fringes corresponds to the (111) direction in the fcc structure. Due to the faceting and random orientation of the particles on the substrate the size distribution as shown in Fig. 4(d) mainly indicates the geometrical features of the nonspherical particles. The distribution function for the number of atoms per particle cannot unambiguously be obtained from these data. Nevertheless, the average spatial dimension is in the order of 4 nm. With respect to a possible core-shell structure<sup>35</sup> in the distribution of Fe and Pt, the TEM images give no indication of such an inhomogeneity. Due to the difference in the scattering cross section between Fe and Pt, a core-shell structure should be easily visible within the spatial resolution of the microscope.<sup>7,3,36,35</sup> Similarly, no oxide shell could be found in any of the analyzed particles.

#### B. Brownian motion

At room temperature, the as prepared particles order in a regular two-dimensional pattern on a flat substrate with an average nearest-neighbor distance of 6 nm [see Fig. 4(a)]. This corresponds to the double chain length of the organic ligands which is approximately 2.8 nm. In the same manner the particles can be ordered and separated in three dimensions.<sup>37</sup> The paramagnetic Mössbauer spectra in Fig. 5

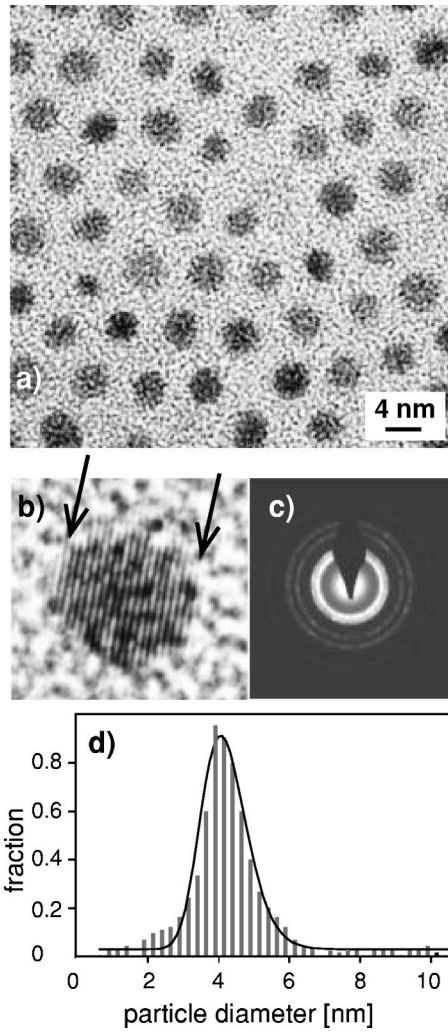


FIG. 4. (a) TEM micrograph demonstrating the self-assembling of the FePt nanoparticles. (b) HRTEM picture of a single nanoparticle. The faceting of the particle is clearly visible. Between the two arrows 20 lattice planes are observable with a lattice spacing equal to that of the  $\langle 111 \rangle$  direction in this system. (c) Small area electron-diffraction pattern of the as-prepared FePt particles. Finally, (d) gives the size distribution for the as-prepared particles.

demonstrate the characteristic line broadening (Fig. 6(a)) in the vicinity of 250 K due to the Brownian motion of the monodisperse (with respect to their mass) particles, thus proving their separation. Surprisingly, the line broadening is accompanied by a steep decrease of the resonant count rate [Fig. 6(b)]. Above 250 K the resonant signal is undetectable. Agglomeration is thus excluded, as it would ensure a resonant signal even at room temperature.

Although the concept of pure Brownian-like diffusion is not likely to be applicable in the case of self-organized particles with a defined average distance of 6 nm, which is in the order of the particle diameter, a mathematical treatment within this framework may reveal some insight into the elastomechanical properties of the ligand-particle system by looking at similarities and systematic deviations with respect to the experimental evidence. Referring to the work of Singwi and Sjölander<sup>38</sup> with respect to thermally activated

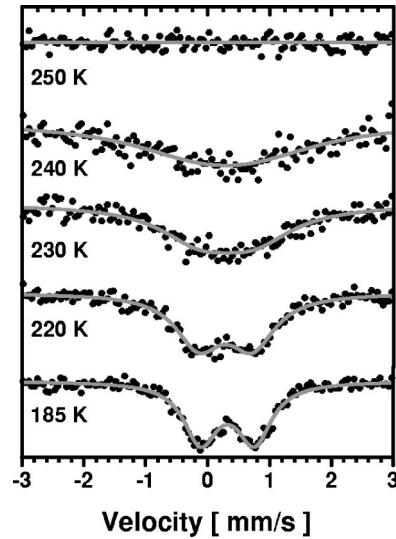


FIG. 5. Line broadening due to Brownian motion of the FePt nanoparticles (batch I).

diffusion Bonchev<sup>39</sup> treated the Mössbauer cross section under the influence of Brownian motion. The line broadening  $\Delta\Gamma$  is given by the expression

$$\Delta\Gamma = 2k^2D \quad (1)$$

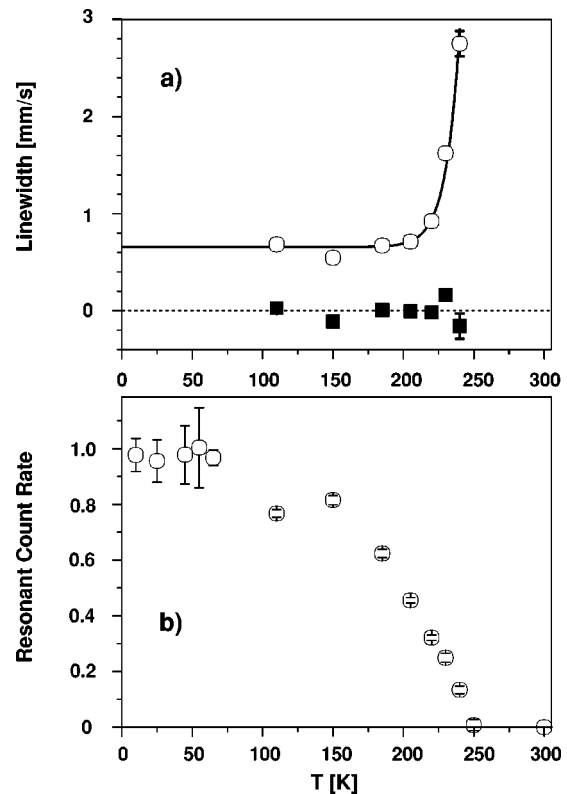


FIG. 6. (a) Linewidth as a function of temperature.  $\circ$ : experiment,  $\blacksquare$ : experiment minus analytical approach. (b) Resonant absorption as a function of temperature. The low-temperature values were set to unity.

with  $D$  the diffusion constant and  $k$  the  $\gamma$ -wave vector. Using the Einstein-Stokes diffusion constant (viscosity  $\eta$ , particle radius  $R$ , Boltzmann constant  $k_B$ ),

$$D = \frac{k_B T}{6\pi\eta R}, \quad (2)$$

the line broadening yields

$$\Delta\Gamma(T) = \frac{k^2 k_B}{3\pi R} \frac{T}{\eta(T)}. \quad (3)$$

The line broadening should be a linear function of  $T/\eta$ . Using these expressions and literature values<sup>40</sup> for  $\eta(T)$  (oleic acid) the least-square fit of the experimental data yields an effective particle diameter of 4 cm which definitely shows the inadequacy of the above approach. This failure is further supported by the rapid decrease of the Debye-Waller factor [Fig. 6(b)] that accompanies the line broadening. This is not expected for pure diffusion.

A modified approach to the experimental data is the consideration of a superlattice<sup>60</sup> of FePt particles with an elastic coupling via the organic ligands that are chemically bound to the particle's surface. In the same way as in a solid lattice the Debye-Waller factor of the particle system can be treated by the vibrational properties of the superlattice. Compared to the situation of a Mössbauer probe atom in a solid lattice there are the following significant differences:

(i) At higher temperatures, i.e., in the limit of free particles, the energy shift due to the  $\gamma$  recoil is determined by the mass of one FePt particle.

(ii) The mechanical coupling between neighboring FePt particles is weak and a strong function of temperature.

(iii) At higher temperatures, the viscous properties of the organic molecules can lead to a nonlinear response to the displacement of the FePt particles from their average positions.

(iv) Local Brownian motion is superimposed on the superlattice vibrations.

Point (i) makes it clear that above 250 K the Debye-Waller factor is practically zero. The recoil energy on a single Fe atom would be 2 meV. The mass ratio between a 4-nm FePt particle and an Fe atom is about 7000, resulting in a recoil energy of 0.3  $\mu$ eV. This is still larger by a factor of 65 than the natural linewidth of 4.6 neV of the <sup>57</sup>Fe Mössbauer transition. Only a mechanical coupling into effective units of at least 100 FePt particles will lead to a measurable resonant absorption. As the temperature is reduced below 250 K, the increasing stiffness of the organic ligands will mediate this coupling. It is clear that a temperature-dependent mechanical correlation length  $\xi(T)$  in the superlattice of the particles will be observed.  $\xi$  defines an ensemble of particles around a central FePt particle that participates in the resonant absorption of a 14.4-keV  $\gamma$  quantum. They provide the necessary effective mass to yield the recoil-free fraction (Debye-Waller factor) in the Mössbauer experiment. Thus the determination of the Debye-Waller factor  $f(T)$  gives experimental access to  $\xi(T)$ , which is linked to the stiffness of the organic molecules.

Since  $\xi$  provides the effective mass in the Mössbauer process it will also define an ensemble of weakly coupled mechanical oscillators. This results in a movement of the Mössbauer active central FePt particle around an average position as a function of time. The average squared displacement will enter into the calculation of the resonant fraction  $f(T)$ :

$$f(T) \sim e^{-k^2 \langle x_{\text{particles}}^2(T) \rangle}, \quad (4)$$

where  $k$  is the wave vector of the  $\gamma$  radiation.

For a treatment of the Mössbauer line broadening that follows the concept of Brownian motion, Eq. (2) has to be reconsidered.  $D$  in this context is the diffusion constant of a (large) object in a viscous medium. The given quantitative relation should break down when the object size (particle) approaches the molecule size (oleic acid) of the medium. In addition, the oleic acid molecules bind as ligands to the particle's surface. The ligands between neighboring particles penetrate and interact with each other. Though Eq. (2) will not hold in a strict sense, the random motion of the particles will be describable by a diffusion constant  $D$  and Eq. (1) is still valid. In a first approach, the general temperature dependence of  $D$  is assumed to still follow Eq. (2), but the physical background has to be reinterpreted. In effect, to describe the viscomechanical properties of the particle-ligand system, we keep the temperature dependence

$$D(T) \sim \frac{T}{\exp\left(-\frac{T}{T_0}\right)} \quad (5)$$

in analogy to the temperature dependence of  $\eta$ .<sup>61</sup>

The experimental linewidth can then be described by the expression

$$\Gamma(T) = A \frac{T}{T_0} \exp\left(\frac{T}{T_0}\right) + \Gamma_0 \quad (6)$$

in analogy to Eq. (3).  $\Gamma_0$  represents the temperature-independent linewidth due to the hyperfine interaction.  $T_0$  is a characteristic temperature for the elastic and viscous properties of the organic coating of the particles and  $A$  is a materials constant. The quantities  $A$ ,  $T_0$ , and  $\Gamma_0$  can be determined by fitting the experimental data. To avoid systematic errors due to the magnetic interaction in the FePt particles at lower temperatures, only experimental values between 185 and 240 K were taken into account. In Fig. 6(a) the result is plotted with the determined parameters  $A = 4.3 \times 10^{-12}$  mm/s,  $T_0 = 10(1)$  K, and  $\Gamma_0 = 0.66(2)$  mm/s.

In summary, the line broadening in the Mössbauer experiment is due to the local motion of the particles. The unphysical result of a particle diameter of 4 cm in a standard approach is related to the altered physics behind the viscous and elastic properties of the particle-ligand system in the dense superlattice compared to a liquid. The rapidly decreasing Debye-Waller factor has to do with the vibrations of the superlattice.

TABLE I. Hyperfine values of the as-prepared samples ( $\Gamma$ : linewidth). \*IS relative to  $\alpha$ -Fe at room temperature (RT), not corrected for the second-order Doppler shift.

$T$	Batch	Component	IS* [mm/s]	QS [mm/s]	$\langle B_{\text{hf}} \rangle$ [T]	$\sigma(B_{\text{hf}})$ [T]	$\Gamma$ [mm/s]
185 K	I		0.43(1)	0.86(2)			0.66(2)
200 K	II		0.43(2)	0.80(2)			0.64(2)
10 K	I	A ( <b>13%</b> )	0.45(3)	-0.06(3)	33.4(2)	0(2)	0.4(1)
	I	B	0.52(2)	0.027(14)	46.5(2)	3.0(2)	0.60(1)
10 K	II	A ( <b>28%</b> )	0.50(4)	-0.04(4)	33.5(3)	0.8(8)	0.79(8)
	II	B	0.48(2)	-0.02(2)	46.2(2)	2.3(3)	0.69(7)

### C. Magnetic properties

Regarding the questions linked to the electronic properties of the FePt particles, Mössbauer spectroscopy gives access to the Fe charge state, the local charge distribution, as well as the magnetic hyperfine field. Table I denotes the hyperfine parameters of two batches in the as prepared state. Without going into detail, the parameters indicate the high reproducibility in the synthesis of the FePt system. The only obvious deviation in the two batches is the ratio between the magnetic components *A* and *B* at 10 K.

At 10 K, the Mössbauer spectra of both batches demonstrate the complete magnetic order (see Fig. 12). The two subspectra *A* and *B* show rather distinct parameters. The hyperfine parameters of component *A* are typical for the ferromagnetic Fe-Pt system. Naively one would expect this fraction to dominate the spectrum, as the core contribution in a 4-nm particle amounts to around 65%. Instead, component *B* is dominant and amounts to 87(2)% and 72(2)% in batch I and II, respectively. The magnetic hyperfine field distribution of component *B* extends to values as large as 50 T which is unusually high. Keeping in mind that we are dealing with a nanostructured material and an alloy system, it should be stressed that the width of the hyperfine field distribution of component *B* at 10 K is rather narrow, especially if compared to literature data of Fe-Pt multilayers.<sup>41–48</sup> The simple Gaussian shape of the  $B_{\text{hf}}$  distribution would be compatible with the disordered fcc phase seen in XRD. Details will be discussed later.

To elucidate the origin of the enhanced magnetic hyperfine field the formation of Fe oxides has to be considered which would easily explain the observed large values.  $\text{Fe}^{2+}$  oxides can be ruled out from the isomer shift values. Unfortunately, a distinction between possible  $\text{Fe}^{3+}$  oxides and metallic phases in the Fe-Pt system seems not possible in a simple way, as the isomer shifts coincide. Therefore a more thorough investigation by magnetization measurements with a superconducting quantum interference device (SQUID) and a vibrating sample magnetometer (VSM) was undertaken. Furthermore, x-ray photo electron spectroscopy (XPS) helped to clarify the Fe and Pt charge states.

Figure 7 shows zero-field-cooled–field-cooled (ZFC-FC) magnetization curves for the as-prepared particles in an external field of 100 G. An absolute calibration of the magnetic moment per particle could not be established for this mea-

surement as the precise determination of the pure particle mass without ligands is as of yet impossible. Clearly visible is the irreversibility in the two magnetization curves which is due to the superparamagnetic behavior. The freezing temperature that is linked to the measuring time of 1 s is determined to be 11.0(5) K (dotted vertical line). In the temperature-dependent Mössbauer data the corresponding value of 55(5) K is linked to the nuclear Larmor precession time of  $1.2 \times 10^{-8}$  s. Assuming a particle diameter of 4 nm and a simple exponential dependence of the superparamagnetic relaxation time on  $KV/k_B T$  ( $K$ : effective magnetic volume anisotropy;  $V$ : particle volume;  $k_B$ : Boltzmann constant;  $T$ : temperature),  $K$  can be estimated to 0.11(3) MJ/m<sup>3</sup>. The determination of the average anisotropy constant from the slope of the mean magnetic hyperfine field as a function of temperature below 50 K yields a value of 0.050(3) MJ/m<sup>3</sup> ( $K \cdot V = 0.009$  eV). The statistical error bars (numbers in parentheses) are a lower limit as systematic errors cannot be disregarded. One has to keep in mind that the above treatment of  $K$  is only valid if the surface anisotropy can be neglected. This is definitely not the case in the present system, as will be shown later. Therefore  $K$  has to be seen as an effective anisotropy value normalized to the particle volume. In addition, the quantification of the relaxation of the collective moment within a single particle depends on the assumption of a rather simple potential of the magnetization in a uniaxial anisotropy field.

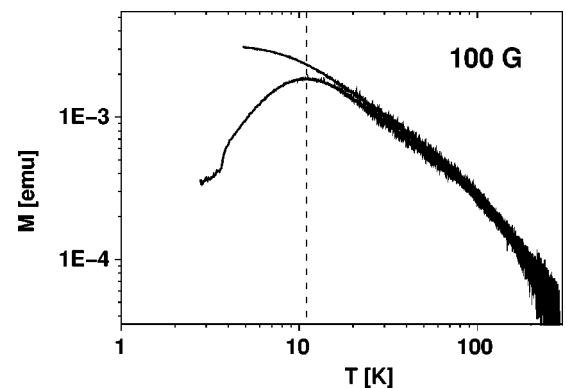


FIG. 7. ZFC-FC magnetization curves in an external field of 100 G for the as-prepared sample (batch II).

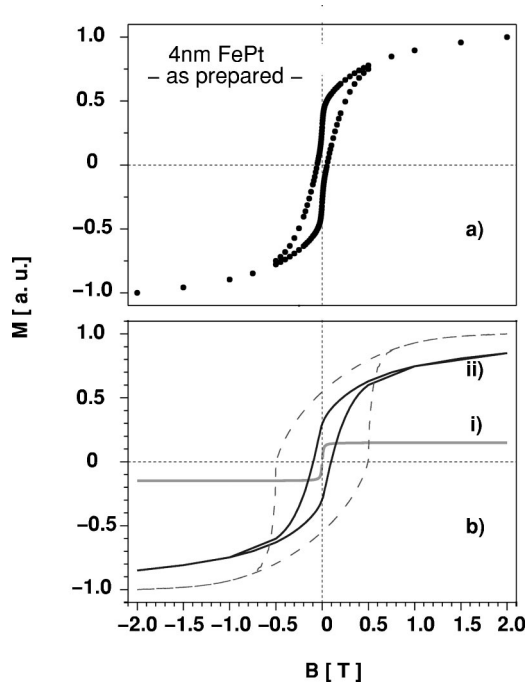


FIG. 8. (a) Hysteresis loop of the as-prepared particles in the organic matrix at 4.3 K measured with a SQUID magnetometer (batch II). (b) Decomposition into a superparamagnetic (i) and blocked fraction (ii) of particles of equal moment. For comparison the dashed line indicates the classical Stoner-Wohlfarth theory.

#### D. Magnetic Hysteresis

TEM, x-ray, and Mössbauer data reveal a highly monodisperse character of the FePt sample with respect to size, magnetic hyperfine field, and crystallinity. In contrast to this uniformity, the hysteresis loop at 4.3 K exhibits a rather complex behavior. To get an idea of the peculiarities one can compare it with a standard Stoner-Wohlfarth system of randomly oriented independent monodisperse uniaxial particles. In Fig. 8(b) the magnetization behavior of such a system as a function of external field is given by the dashed line. The characteristics are: (i) The point of steepest slope is at the coercive field, that is a strong increase of  $|M|$  into the opposite direction as before occurs here. (ii) Saturation is only gradually approached. (iii) Remanence is in the order of half the saturation magnetization. (iv) The slope at zero external field shows a value intermediate between the steepest part of the magnetization curve and saturation.

On a rough evaluation, the measured magnetization curve of the FePt particles shows the following differences: The steepest descent is around zero external field leading directly into the gradual approach of the saturation magnetization, even before  $M$  reverses sign. The intermediate value of the slope is seen here at the coercive field instead of zero external field.

This contrasting behavior has to be related to the anisotropy properties of the particles or cooperative effects, as the particle size is definitely well defined (supported by small-angle x-ray scattering data<sup>49</sup>). The moment per particle should be as monodisperse as the electronic properties. The indirect magnetic coupling between the particles by dipolar

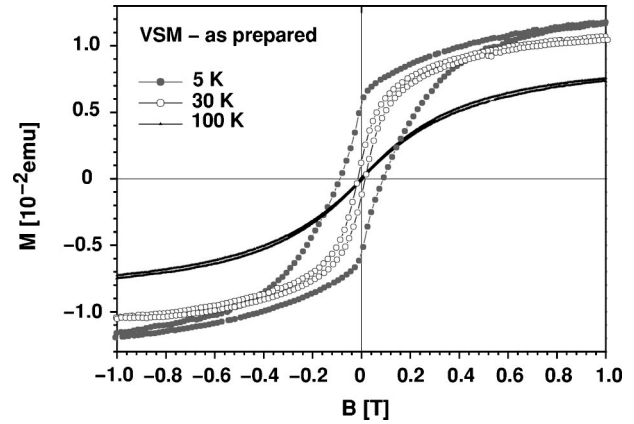


FIG. 9. Hysteresis loops of the as prepared particles in the vibrating sample magnetometer at 5, 30 and 100 K (batch II).

interaction is certainly a point to be carefully looked at as the particle-particle distance is of the order of the particle size. This could explain a collective switching at low fields but it remains unclear how this could be reconciled with the observation that  $M$  does not change sign close to the steepest part of the magnetization curve.

Further insight is gained if one takes into account the following crude decomposition of the magnetic hysteresis loop into two possible contributions. In spite of the monodisperse character of the particles, a superposition of a superparamagnetic (i) and a magnetically blocked (ii) fraction as indicated in Fig. 8(b) could reproduce the measured hysteresis loop. If one considers a distribution of anisotropy constants then this bimodal behavior [(i) and (ii)] no longer seems artificial. Fraction (ii) is made up by those particles that have an anisotropy constant above a critical range and are thus blocked. Fraction (i) on the other hand is made up of those particles with a lower anisotropy constant than this range and are fully superparamagnetic. The fraction of particles within the critical range is small, as the thermal activation depends exponentially on the ratio of anisotropy to thermal energy. The critical range can be shifted either by raising the temperature or by changing the anisotropy distribution. The first case is seen in Fig. 9, where at 30 K most of the particles become superparamagnetic, i.e., belong to fraction (i). The second case will be discussed later in the section dealing with annealing experiments and can be seen in Fig. 13. There it will be demonstrated that surface anisotropy plays a crucial role in the FePt nanosystem. In this light it is clear that the above suggestions can only give an impression of the complexity of the switching dynamics. The origin of the magnetization behavior lies in the surface anisotropy field of each particle. The route of magnetization reversal along the surface of a particle follows local minima and lacks the simplicity of uniaxial symmetry.

Further remarks on the switching behavior in Fig. 9 are the following: In the Stoner-Wohlfarth case with a certain size distribution the (super)paramagnetic fraction is usually attributed to small particles that can be aligned only in larger fields. The related saturation field will increase with increasing temperature. In the present case the seemingly paramagnetic fraction (i) is most easily magnetized along the external

field direction whereas the slope at the coercivity field for fraction (ii) is significantly smaller. The same systematics is seen in the temperature dependence of the hysteresis loop. An increase in temperature from 5 to 30 K helps to overcome the magnetic anisotropy whereas the thermal fluctuations of the collective moments are still moderate. Thus the maximum slope of the magnetization curve increases and the coercivity notably reduces while the magnetization value at 1 T stays nearly the same. Sticking to simple decomposition into fractions (i) and (ii), the equal magnetic field energy has to compete against thermal agitation in both cases but in case (ii) the magnetic anisotropy has to be overcome additionally. Thus the particles with nonvanishing anisotropy show hysteresis and a stretched out magnetization curve along the external field axis. At higher temperatures the usual decrease of the average moment and an increase of the saturation field due to thermal fluctuations is observed.

In conclusion, the measured magnetization curve in Fig. 8(a) is a superposition of contributions from an ensemble of monodisperse particles with identical magnetic moment but a wide distribution of magnetic anisotropy values and characteristics. A significant fraction exhibits practically zero anisotropy. In a simplified picture, a paramagnetic and a hysteretic fraction can account for the observed hysteresis measurements. The finite slope of the magnetization curve at high fields (1–2 T) is an indication of spin canting at the particle's surface. This is in agreement with the concept of surface anisotropy. A further insight into the nature of the anisotropy will be discussed on the basis of the results for the annealed samples.

### E. Electronic properties

To further confirm the (mainly) metallic character of the FePt nanoparticles XPS measurements were undertaken. Silicon covered by a thin natural oxide layer was used as a substrate. After coating the substrate with a droplet of the

dispersion, a self-organized monolayer of FePt particles readily formed. This was checked by TEM imaging using amorphous carbon as substrate. XPS spectra were recorded at the characteristic photoenergies of C 1s, Fe 2p, and Pt 4f (Fig. 10).

For Fe as well as Pt two components are found: The neutral state at binding energies of 708 and 71.2 eV, respectively, and a nonzero charge state at 711.3 and 72.3 eV. The relative contributions of both components to the spectra are not identical for Fe (73% and 27%) and Pt (82% and 18%). An overall energy shift of the spectra compared to reference data of bulk standards is due to initial- and final-state effects of the electron emission process in small particles.<sup>50</sup> The mainly metallic nature of the particles is further proven by the nonvanishing density of states (DOS) at the Fermi level probed with the same XPS method. Details on these results will be given in a forthcoming publication focusing on the electronic structure of the FePt particles.<sup>51</sup>

### F. Annealing experiments

To learn more about the crystallographic, morphological, and chemical stability of the particle-ligand system the FePt particles were heat treated in ultrahigh vacuum ( $10^{-8}$  mbar) at 350 and 560 °C for 30 min. The warming up as well as the cooling down phase took 2 h each. The first annealing step was chosen to gently decompose the organic shell of the particles. Close to 350 °C the organic matrix shows a characteristic mass loss. This results in an outgassing of hydrogen and oxygen components whereas carbon is mainly left as a residue. The second annealing step at 560 °C was chosen as a change in the crystal structure of the FePt particles was expected.

The XPS measurements of the heat treated samples do not show drastic changes in the charge state of the Fe and Pt atoms. This is demonstrated in Fig. 10 at the Fe-2p and the Pt-4f edges. Obviously, neither the main metallic component

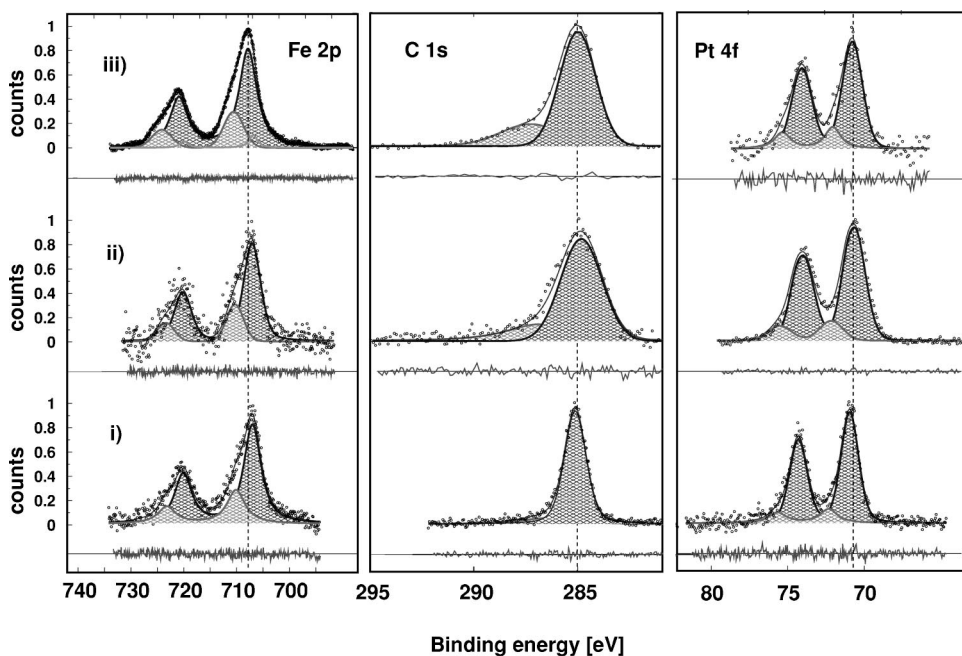


FIG. 10. C, Fe, Pt photoelectron spectra of the as-prepared (i) and heat treated (ii: 350 °C; iii: 560 °C) samples (batch II).

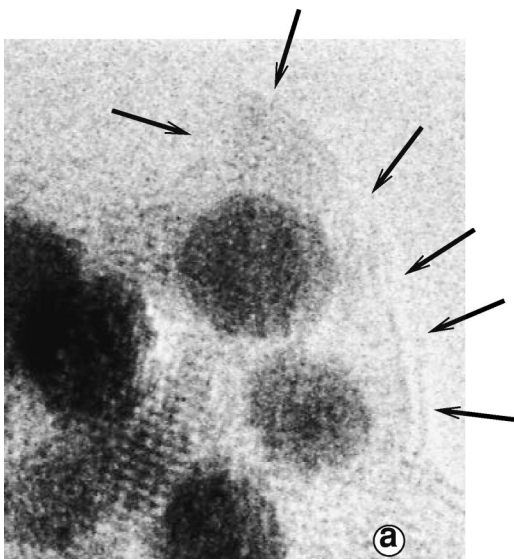


FIG. 11. High-resolution TEM image of the sample annealed at 560 °C. Arrows indicate the carbon shell covering the particles.

nor the minor component attributed to a nonzero charge state change significantly in relative intensity.

Nevertheless, the XPS signal at the C-1s edge reveals the changes in the shell of the FePt particles. The evolution of a second component at higher binding energies relative to the main carbon peak can be attributed to the reaction of C with the particle's surface. This is clearly seen in the  $^{57}\text{Fe}$ -Mössbauer spectra as will be discussed later. The high-resolution TEM measurement in Fig. 11 shows the existence of a shell of carbonous material around the nanoparticles. This shell formation might be enhanced during annealing due to a possible catalytic action of the FePt surface.<sup>52</sup>

In electron diffraction no changes are observed in the line pattern. This proves the stability of the fcc phase up to temperatures as high as 560 °C with annealing times of 30 min. However, a diffuse scattering background develops during this treatment. Most probably, this additional signal originates from the carbon or Fe-Pt-C compound shell covering the particles. The stability of the fcc phase is also confirmed by x-ray diffraction (XRD). It is worth mentioning that no agglomeration or particle growth is observed compared to the as-prepared state. The width of the diffraction peaks remains unchanged.

In summary, the heat treatment at temperatures of 350 and 560 °C leads primarily to the decomposition of the surfactant and in a second step to the formation of an amorphous or nanocrystalline shell of carbon and Fe-Pt-C compounds. Though the annealing process was undertaken in ultrahigh vacuum oxygen may be present in the surface region of the particles. Mössbauer measurements further clarify the surface chemistry.

Figure 12 shows the Mössbauer spectra of the (i) as prepared, annealed at (ii) 350 °C and (iii) 560 °C samples measured at 10 K. Spectrum (iii) exhibits differences mainly in the central part compared to spectrum (i). This is linked to the Fe-Pt-C compound formation at elevated temperatures, leaving the core of the particle in its original metallic state.

Spectrum (ii) seems to be dramatically different to the other two cases. A closer look at the data reveals that the spectrum decomposes into a paramagnetic and a magnetic fraction. The hyperfine parameters of the magnetic fraction are close to those of the as-prepared state. The average hyperfine field is reduced by 6%. The obvious difference to the as-prepared state is given by the central paramagnetic doublet. This indicates that the superparamagnetic blocking temperature for the majority of particles has decreased from an initial value of 55 K to below 10 K after the first gentle annealing step. The paramagnetic fraction of 71% in the Mössbauer spectrum equals the increase of the (super)paramagnetic fraction in the low-field part of the hysteresis curve at 4.3 K in Fig. 13. As the particle size has not changed according to the TEM results, the reason for the drop of the blocking temperature lies in a respective reduction of the magnetic anisotropy  $K$  in these particles.

As XRD and small area electron diffraction (SAED) data exclude a significant change in the crystal structure, the only possible origin of the change in  $K$  must be attributed to the surface of the particles. This is consistent with the fact that for the observed cubic structure of the disordered FePt alloy one would expect a low magnetocrystalline (volume) anisotropy. Thus the decomposition of the organic ligands that starts at 350 °C changes the surface state of the metallic particles. It is most likely that the oleic acid molecules bind via the double bonded O to Fe surface atoms. This is reflected in the higher fraction of nonmetallic Fe compared to nonmetallic Pt in Fig. 10. As the synthesis was undertaken in a non-aqueous solvent a binding via the OH group as discussed in Ref. 53 is not probable. Thermal decomposition breaks up these O-Fe bonds and the entire organic molecules, leaving

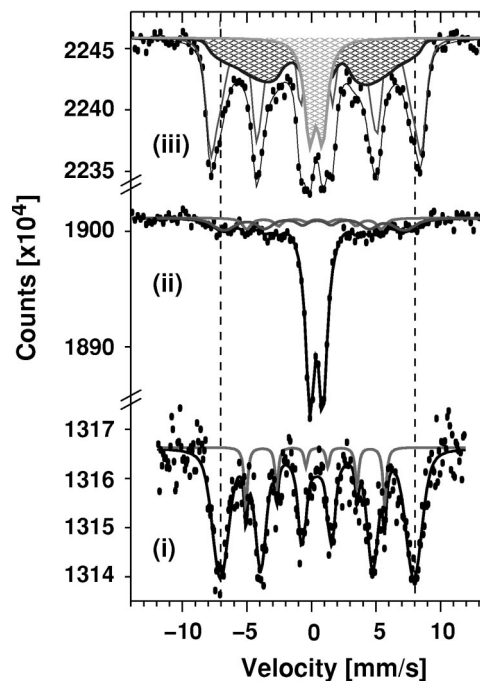


FIG. 12. Mössbauer spectra at 10 K of the (i) as-prepared state (batch I), (ii) annealed at 350 °C (batch II), (iii) annealed at 560 °C (batch II).

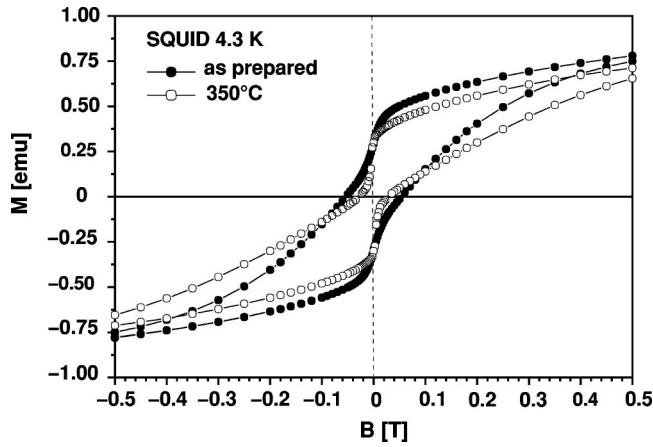


FIG. 13. Hysteresis loops of the particles in the as prepared and first annealed state (350 °C) at 4.3 K normalized to the magnetization at a field of 2 T (batch II).

pure carbon as a matrix for the still separated FePt particles. As a result, the surface anisotropy drops to such an extent that the blocking temperature in the Mössbauer experiment is reduced below 10 K. A similar mechanism for the magnetic anisotropy of a single Co nanoparticles in a Nb matrix was proposed to be induced by the Co-Nb interface in Ref. 54. An increase of the magnetic anisotropy energy constant with decreasing particles size was reported in Ref. 55 for pure Fe particles in vacuum. In our case, using the values for the anisotropy energy and the size of the as-prepared particles the average surface anisotropy can be estimated to about  $10^{-4}$  J/m<sup>2</sup>. At higher annealing temperatures, i.e., at 560 °C in the present experiment, the activation energy for the formation of a shell of Fe-Pt-C compounds is overcome. As a result, the higher magnetic anisotropy is regained. Though the XRD results show a further reduction of the lattice constants the fcc structure is preserved.

To summarize the Mössbauer results, Fig. 14 shows the hyperfine field distributions at 10 K for the different samples and preparation steps. The paramagnetic contributions at  $B_{\text{hf}}=0$  T are not shown. The slightly reduced  $B_{\text{hf}}$  scale in the annealed state (ii) compared to the as prepared samples could either be explained by the relaxation of the collective moment of the particles, as a complete blocking of the mo-

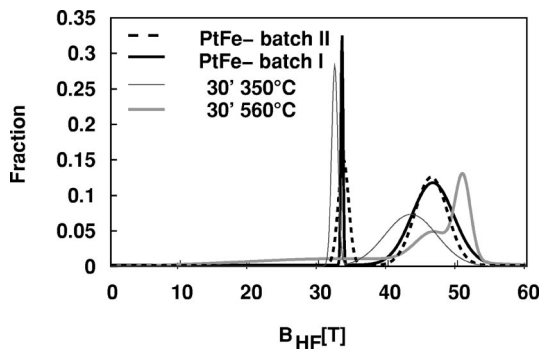


FIG. 14. Hyperfine field distributions of the two batches in the as prepared state and of the second batch annealed at 350 °C and 560 °C.

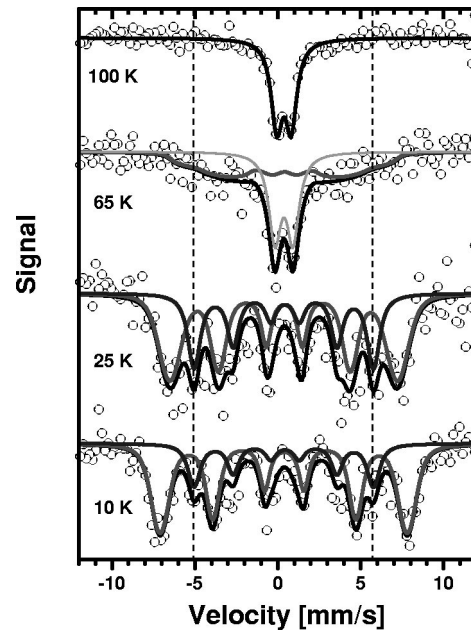


FIG. 15. Mössbauer spectra of batch II in the as-prepared state between 10 and 100 K.

ments is not reached, yet (similar to the as-prepared state at 65 K in Fig. 15). On the other hand, it might reflect a change in the electronic structure.

In the annealed state (iii) the magnetic component with the well-defined hyperfine field of 33.5 T vanishes. Instead, contributions over a broad range of hyperfine fields from 10 to 40 T appear in the spectrum (component *D* in Table II, 34%). They have their origin in the formation of Fe-Pt-C compounds at the surface (component *C* in Table II, 17%), resulting in a core-shell structure of the particles. The core of the FePt particles (49%) appears unchanged with respect to the range of the observable hyperfine fields between 40 and 55 T and the related isomer shift. Nevertheless, the weight of this part of the hyperfine field distribution is shifted towards higher values in  $B_{\text{hf}}$ . This sheds light on the possible mechanism for these enhanced hyperfine fields as the effective size of the metallic FePt core shrinks due to the formation of the Fe-Pt-C compound shell with its strong chemical bonds.

In summary, what is seen in Fig. 14 is the response of the electronic system in the core of the particles to the changes in chemical bonding of the outer atomic layer(s) when going through the states (i)–(iii). The detailed hyperfine parameters are given in Table II.

#### IV. DISCUSSION AND OUTLOOK

The reported experimental findings concerning 4-nm FePt particles reveal a set of unpredicted features for a metallic system of that size. With about 3000 atoms, these particles should closely approach bulk properties. Deviations are expected to originate from the surface and the chemical bonding of the organic ligand molecules to the nanoparticles. However, the above observations in the as-prepared as well as annealed states cannot be explained in this simple picture.

TABLE II. Hyperfine values of the annealed samples (batch II)—(ii): annealed at 350 °C and (iii): annealed at 560 °. \*IS relative to  $\alpha$ -Fe at RT, not corrected for the second-order Doppler shift.

	State	Component	IS* [mm/s]	QS [mm/s]	$\langle B_{\text{hf}} \rangle$ [T]	$\sigma(B_{\text{hf}})$ [T]	$\Gamma$ [mm/s]
At 10 K	(ii)	A[9(2)%]	0.43(9)	-0.12(8)	32.3(1.7)	0.2(2)	0.9(4)
	(ii)	B[20(2)%]	0.41(12)	-0.1(1)	43.5(1.6)	3.4(8)	0.7(4)
	(ii)	C[71(2)%]	0.49(1)	0.97(2)			0.75(3)
At 10 K	(iii)	B-1 [26(1)%]	0.49(1)	-0.03(1)	50.8(2)	1.1(3)	0.62(6)
	(iii)	B-2 [23(1)%]	0.46(2)	-0.01(2)	46.5(6)	2.6(1)	0.50(8)
	(iii)	C[17(1)%]	0.46(2)	1.00(4)			0.93(6)
	(iii)	D [34(1)%]	0.47(5)	-0.10(5)	34.1(6)	14.8(2.3)	0.50(5)

The following features are the essential results of the experiments reported:

(i) The crystal structure of the as-prepared system is fcc, resembling the high-temperature phase of the Fe<sub>50</sub>Pt<sub>50</sub> alloy. The lattice constant of 0.3839 nm is in perfect agreement with an Fe-Pt alloy of an Fe content of 50%. This is in agreement with the RBS results. There is no direct experimental clue, whether Fe and Pt form a regular structure or whether the disordered high-temperature phase is realized. Nevertheless, the vanishing magnetic anisotropy of the core and the missing superlattice peaks in XRD and SAED give strong evidence of the disordered state.

(ii) Even after the annealing step at 560 °C the envisaged fct room-temperature phase is not formed. Only a change of the lattice parameters is observed. Agglomeration and particle growth can be ruled out.

(iii) The XPS data of the Fe core levels clearly show that the majority of the Fe atoms are in a neutral charge state. Considering the valence-band density of states close to the Fermi energy a metallic character of the particles is proven. The as-prepared FePt nanoparticles are inert to oxidation in air, which is in contrast to observations of pure Fe, Ni, or Co particles of the same size. Those are instantly (within milliseconds) covered by an oxide shell.<sup>3</sup> The presence of Pt crucially contributes to the chemical inertness.

(iv) The electric quadrupole splitting (QS) as well as the magnetic hyperfine field  $B_{\text{hf}}$  exhibit values that are surprisingly high for the metallic FePt system. Considering the results of the sample characterization with XPS, XRD, SQUID magnetization, and TEM in conjunction with the complex annealing behavior a trivial explanation by Fe oxides at the particle's surface must be ruled out.

(v) The measured low magnetic anisotropy of  $\approx 0.1$  MJ/m<sup>3</sup> of the FePt particle system has its origin in surface contributions. The surface anisotropy depends on the chemistry of the particles with the surrounding matrix. Fe oxides can be ruled out in this context as they would be stable against the performed heat treatment and should exhibit a dominating volume anisotropy.

(vi) The Brownian motion of the FePt particles characterizes the temperature-dependent viscous properties of the organic ligand system.

The peculiar properties of the as-prepared 4-nm FePt particles manifest themselves in a reduction of 1% of the lattice

constant compared to quenched bulk samples, in an enhanced magnetic hyperfine field<sup>56</sup> and electric quadrupole splitting and in a zero magnetic anisotropy of the core. The electric quadrupole splitting is a direct evidence of the local anisotropy<sup>62</sup> of the charge distribution around the Fe atoms. The polarization of the Fe atomic shell is certainly related to a local magnetic anisotropy. For a random distribution of Fe and Pt on the fcc lattice sites this anisotropy will vary statistically in size and direction. The resulting magnetic anisotropy of the particle's core averages to zero in the same way as in soft-magnetic amorphous or nanocrystalline materials. This explains the strong paramagnetic signal in the Mössbauer and magnetization measurements at low temperatures in the absence of surface anisotropy (first annealing state).

Regarding the homogeneity of the FePt system the hyperfine interaction gives some additional information. At 10 K, the Mössbauer spectra consist of two distinct magnetic components. In batch I the regular component A amounts to 13%, in batch II to 28%. The average size and the rather sharp distribution of its magnetic hyperfine field would be in accordance with the expected ordered fct phase.<sup>56</sup> This phase should have the large magnetocrystalline anisotropy which is the basis for the interest in the FePt system. From the bimodal hyperfine field distribution one is tempted to suggest the occurrence of two kinds of particles: one in the disordered fcc phase and the other in the ordered fct phase. Looking at the temperature dependence of both Mössbauer signals in Fig. 15 this assumption is ruled out. If two separate types of particles were present in this measurement they would exhibit two well distinguished blocking temperatures according to the differences in magnetic anisotropy. Especially, component A (indicated by dashed vertical lines) should show magnetic ordering far above the paramagnetic collapse of component B. This is not the case. The magnetic ordering of component A collapses in the same way as component B. A similar argument holds for the relative intensities of both components in the as-prepared and the first annealed state (350 °C). As was discussed earlier, this moderate annealing step mainly decreases the surface anisotropy contribution. As the magnetocrystalline anisotropy in the fct system should exceed the surface anisotropy significantly, such a heat treatment would not affect the magnetic ordering of such particles. Thus only in particles of fcc structure a collapse to the paramagnetic state would be seen. The A-B ratio would

change accordingly. On the contrary, the intensity ratio between the magnetically ordered components *A* and *B* of roughly 1:2 is the same in the as-prepared and annealed sample at 10 K.

In the same way, the simultaneous occurrence of metallic and oxidic particles is ruled out. First of all, the whole sample takes part in the line broadening effect and the reduction of the Debye-Waller factor in the narrow temperature interval from 185 to 250 K. Second, the superparamagnetic blocking temperatures coincide for all components present in the Mössbauer spectra.

Regarding the XRD and TEM results of the as-prepared state, no indication of the fct phase is seen. Thus large fct volume fractions cannot be present in the particles. Mössbauer spectroscopy as a local probe method could still yield the hyperfine interaction of a locally occurring fct-like structure, but this kind of structural variation is unlikely in an itinerant magnetic system.

As to the origin of the enhanced magnetic hyperfine field in the Mössbauer spectra at low temperatures, a simple picture cannot account for the observed properties. Similar large hyperfine fields in metallic particles were reported for FePt (Ref. 57) and AuFe.<sup>58</sup> In spite of the peculiarity of the findings no discussion of the results is given.

Points (iii) and (iv) of the discussion indicate a charge transfer from Fe to Pt. This is not in accordance to calculations on small Fe-Pt clusters with up to 309 atoms in Ref. 59 but in agreement with a general trend at Fe-Pt interfaces.<sup>41</sup> The electronegativity of Pt in the nanoparticle system will be accompanied by a reduced reactivity in an atmosphere containing molecular oxygen. Only the reactive environment of an oxygen plasma leads to a complete oxidation of the particles.<sup>51</sup> Nevertheless, the strongly covalent character of the Fe-Pt bond cannot account for the observed large magnetic hyperfine fields. This was experimentally confirmed in multilayer structures.<sup>43,46</sup>

In pure 4-nm Fe particles that were handled under vacuum, Bødker *et al.* observed a monolayer of Fe oxide with peculiar properties.<sup>55</sup> They report an increased hyperfine field of 47.2 T in conjunction with an unusual ferromagnetic behavior. This phase amounts to 10–20%. At first glance our observations fit into the same category. Yet, the relative amounts of fraction *A* and *B* in the Mössbauer spectra according to Table I cannot be explained in this way. For our 4-nm particles we expect a surface contribution of roughly 30%. The nonmetallic fraction in the XPS data is in agreement with this surface contribution. Nonetheless, component *B* in the Mössbauer data that could be related to a surface layer amounts to 85%. The unexpected dominance of component *B* could be explained by a polarization of the electronic states of the conduction electrons in the metallic

core induced by the surface shell. This could be facilitated by the concentric geometry of the system which distinguishes it from multilayer structures. The contribution of the orbital momentum to the magnetic hyperfine field is not yet clarified but the three-dimensional confinement of the electronic system to an effective size that is smaller than the geometric particle diameter due to the chemical shell of surfactants has to be considered. X-ray magnetic circular dichroism experiments are presently being carried out.

## V. CONCLUSION

The structural disorder, the strong covalent character of the Fe-Pt bond, the influence of the organic ligand system, and the confinement to less than 4 nm lead to electronic properties which are not yet fully understood but justify the strong efforts in the experimental field. Most striking is the enhanced magnetic hyperfine field that is observed at 10 K. A simple oxidation of the particles as a whole or of a significant part of their surface is ruled out. For the interpretation of the hyperfine interaction one has to keep in mind that the electronic wave function is directly probed at the sites of the Fe nuclei. This is quite different information compared to the density of states that is probed by the XPS method. Furthermore, due to the complicated interplay of the *s*, *p*, and *d* states in an itinerant system of finite size, polarization effects on the Fe core states not seen in bulk samples can obscure the situation. Thus, for instance, a direct conclusion on the magnetic moment of the Fe atoms cannot be drawn from the observation of the enhanced magnetic hyperfine field. Nonetheless, the measured hyperfine parameters will be a crucial quantitative test for a theoretical treatment of the FePt nano-system.

The clear evidence of surface anisotropy in the FePt nanoparticles poses the question of its chemical origin with respect to the organic ligands or the carbon matrix. In future applications a proper choice of the surface chemistry might allow a tuning of the magnetic anisotropy properties of small metallic particles. To clarify the character of the magnetic ordering in greater detail, Mössbauer measurements in external fields and neutron diffraction will be carried out.

## ACKNOWLEDGMENTS

We thank the Center for Functional Nanostructures Karlsruhe (CFN) and the Deutsche Forschungsgemeinschaft (DFG) for financial support. We thank the Institute for Nanotechnology Karlsruhe (INT) and the Materials Science Department at the University of Technology Darmstadt for the challenging scientific atmosphere and the spirit of cooperation.

\*Also at Institut für Nanotechnologie, Forschungszentrum Karlsruhe, D-76021 Karlsruhe, Germany. Electronic address: branko.stahl@hrzpub.tu-darmstadt.de

<sup>1</sup>Y. Jo and K. Lee, *J. Magn. Mater.* **226-230**, 1045 (2001).

<sup>2</sup>K. Lee, J. Callaway, and S. Dhar, *Phys. Rev. B* **30**, 1724 (1984).

<sup>3</sup>P. Mulvaney, *MRS Bull.* **26**, 1009 (2001).

<sup>4</sup>U. Kreibitz and M. Vollmer, *Optical Properties of Metal Clusters* (Springer-Verlag, Berlin, 1996).

<sup>5</sup>A. Stella, M. Nisoli, S. D. Silvestri, O. Svelto, G. Lanzani, P. Cheyssac, and R. Kofman, *Phys. Rev. B* **53**, 15 497 (1996).

<sup>6</sup>R. C. Baetzold, *Surf. Sci.* **106**, 243 (1981).

<sup>7</sup>G. Schmid, *Chem. Rev.* **92**, 1709 (1992).

- <sup>8</sup>M. Zhao and R. M. Crooks, *Adv. Mater.* **11**, 217 (1999).
- <sup>9</sup>F. Caruso, *Adv. Mater.* **13**, 11 (2001).
- <sup>10</sup>G. Kataby, Y. Kolytyn, J. Rothe, J. Hormes, I. Felner, X. Cao, and A. Gedanken, *Thin Solid Films* **333**, 41 (1998).
- <sup>11</sup>W. H. Meiklejohn and C. P. Bean, *Phys. Rev.* **105**, 904 (1957).
- <sup>12</sup>J. S. Kouvel, C. D. Graham, and I. S. Jacobs, *J. Phys. Radium* **20**, 198 (1959).
- <sup>13</sup>B. K. Rao and P. Jena, *J. Chem. Phys.* **116**, 1343 (2002).
- <sup>14</sup>B. V. Reddy, S. N. Khanna, and B. I. Dunlap, *Phys. Rev. Lett.* **70**, 3323 (1993).
- <sup>15</sup>J. J. van der Klink, *Z. Phys. D: At., Mol. Clusters* **12**, 327 (1989).
- <sup>16</sup>G. Schön and U. Simon, *Colloid Polym. Sci.* **273**, 101 (1995).
- <sup>17</sup>G. Schön and U. Simon, *Colloid Polym. Sci.* **273**, 202 (1995).
- <sup>18</sup>G. Schmid, R. Pfeil, R. Boese, F. Bandermann, S. Meyer, G. H. M. Calis, and J. W. A. van der Velden, *Chem. Ber.* **114**, 3634 (1981).
- <sup>19</sup>H. H. A. Smit, R. C. Thiel, L. J. de Jongh, G. Schmid, and N. Klein, *Solid State Commun.* **65**, 915 (1988).
- <sup>20</sup>H. G. Boyen, G. Kästle, F. Weigl, P. Ziemann, G. Schmid, M. G. Garnier, and P. Oelhafen, *Phys. Rev. Lett.* **87**, 276401 (2001).
- <sup>21</sup>S. E. Apse, J. W. Emmert, J. Deng, and L. A. Bloomfield, *Phys. Rev. Lett.* **76**, 1441 (1996).
- <sup>22</sup>I. M. L. Billas, J. A. Becker, A. Chatelain, and W. A. de Heer, *Phys. Rev. Lett.* **71**, 4067 (1993).
- <sup>23</sup>I. M. L. Billas, A. Chatelain, and W. A. de Heer, *J. Magn. Magn. Mater.* **168**, 64 (1997).
- <sup>24</sup>G. M. Pastor, J. Dorantes-Davila, and K. H. Bennemann, *Phys. Rev. B* **40**, 7642 (1989).
- <sup>25</sup>J. P. Bucher, D. C. Douglass, and L. A. Bloomfield, *Phys. Rev. Lett.* **66**, 3052 (1991).
- <sup>26</sup>A. J. Cox, J. G. Louderback, and L. A. Bloomfield, *Phys. Rev. Lett.* **71**, 923 (1993).
- <sup>27</sup>R. Galicia, *Rev. Mex. Fis.* **32**, 51 (1985).
- <sup>28</sup>S. M. Dubiel, *Phys. Rev. B* **37**, 1429 (1988).
- <sup>29</sup>B. Stahl, J. Ellrich, N. S. Gajbhiye, G. Wilde, D. Kramer, M. Ghafari, H. Hahn, H. Gleiter, J. Weissmüller, R. Würschum, and P. Schlossmacher, *Adv. Mater.* **14**, 24 (2002).
- <sup>30</sup>A. Buyrn, L. Grodzins, N. A. Blum, and J. Wulff, *Phys. Rev.* **163**, 286 (1967).
- <sup>31</sup>S. Sun, C. B. Murray, D. Weller, L. Folks, and A. Moser, *Science* **287**, 1989 (2000).
- <sup>32</sup>F. Fiévet, J. P. Lagier, and M. Figlarz, *MRS Bull.* **14**, 29 (1989).
- <sup>33</sup>K. Watanabe and H. Masumoto, *Trans. Jpn. Inst. Met.* **24**, (1983).
- <sup>34</sup>H. Okamoto, in *Binary Phase Diagrams* (ASM International, Cleveland, OH, 1996).
- <sup>35</sup>J. I. Park and J. Cheon, *J. Am. Chem. Soc.* **123**, 5743 (2001).
- <sup>36</sup>C. J. O'Connor, J. A. Sims, A. Kumbhar, V. L. Kolesnichenko, W. L. Zhou, and J. A. Wiemann, *J. Magn. Magn. Mater.* **226-230**, 1915 (2001).
- <sup>37</sup>E. Shevchenko, D. Talapin, A. Kornowski, F. Wiekhorst, J. Kotzler, M. Haase, A. Rogach, and H. Weller, *Adv. Mater.* **14**, 287 (2002).
- <sup>38</sup>K. S. Singwi and A. Sjölander, *Phys. Rev.* **120**, 1093 (1960).
- <sup>39</sup>T. Bonchev, P. Aidemirslei, I. Mandzhukov, N. Nedyalkova, B. Skorchev, and A. Strigacher, *Zh. Eksp. Teor. Fiz.* **50**, 62 (1966) [*Sov. Phys. JETP* **23**, 42 (1966)].
- <sup>40</sup>G. H. Eduljee and A. P. Boyes, *J. Chem. Eng. Data* **25**, 249 (1980).
- <sup>41</sup>R. Wu, L. Chen, and N. Kioussis, *J. Appl. Phys.* **79**, 4783 (1996).
- <sup>42</sup>R. Brand, O. Bohné, and W. Keune, *J. Magn. Magn. Mater.* **104-107**, 1891 (1992).
- <sup>43</sup>E. Devlin, V. Psycharis, A. Kostikas, A. Simopoulos, D. Niarchos, A. Jankowski, T. Tsakalagos, H. Wan, and G. Hadjipanayis, *J. Magn. Magn. Mater.* **120**, 236 (1993).
- <sup>44</sup>A. Simopoulos, E. Devlin, A. Kostikas, A. Jankowski, M. Croft, and T. Tsakalagos, *Phys. Rev. B* **54**, 9931 (1996).
- <sup>45</sup>T. Shinjo and W. Keune, *J. Magn. Magn. Mater.* **200**, 598 (1999).
- <sup>46</sup>A. Fnidiki, J. S. Douheret, J. Teillet, H. Lassri, and R. Krishan, *J. Magn. Magn. Mater.* **156**, 41 (1996).
- <sup>47</sup>H. Lassri, M. Abid, R. Krishan, A. Fnidiki, and J. Teillet, *J. Magn. Magn. Mater.* **172**, 61 (1997).
- <sup>48</sup>Y. V. Baldokhin, P. Y. Kolotykin, Y. I. Petrov, and E. A. Shafraunovskiy, *J. Appl. Phys.* **82**, 3042 (1997).
- <sup>49</sup>K. Foster (unpublished).
- <sup>50</sup>G. K. Wertheim, *Z. Phys. D: At., Mol. Clusters* **12**, 319 (1989).
- <sup>51</sup>H. G. Boyen *et al.* (unpublished).
- <sup>52</sup>B. Rellinghaus, S. Stappert, M. Acet, and E. F. Wassermann, *Mater. Res. Soc. Symp. Proc. No. 705* (MRS, Pittsburgh, 2001).
- <sup>53</sup>R. Hirschl, F. Delbecq, Ph. Sautet, and J. Hafner, *Phys. Rev. B* **66**, 155438 (2002).
- <sup>54</sup>M. Jamet, V. Dupuis, C. Thirion, W. Wernsdorfer, P. Mélinon, and A. Perez, *Scr. Mater.* **44**, 1371 (2001).
- <sup>55</sup>F. Bødker, S. Mørup, and S. Linderorth, *Phys. Rev. Lett.* **72**, 282 (1994).
- <sup>56</sup>J. G. Na, *J. Mater. Sci. Lett.* **19**, 1171 (2000).
- <sup>57</sup>M. Tillbrook, Ph.D. thesis, Dept. of Physics, University of Western Australia, 2001.
- <sup>58</sup>P. M. Paulus, H. Bönemann, A. M. van der Kraan, F. Luis, J. Sinzig, and L. J. de Jongh, *Eur. Phys. J. D* **9**, 501 (1999).
- <sup>59</sup>A. Fortunelli and A. M. Velasco, *J. Mol. Struct.: THEOCHEM* **528**, 1 (2000).
- <sup>60</sup>The simple case of a perfect superlattice is not necessarily realized in the present experiment but this is not a vital restriction to the present treatment.
- <sup>61</sup> $\eta(T) = \eta_0 \exp(-T/T_0)$ .
- <sup>62</sup>Deviation from cubic symmetry.